Journal of Alloys and Compounds 902 (2022) 163141

Contents lists available at ScienceDirect

Journal of Alloys and Compounds

journal homepage: www.elsevier.com/locate/jalcom

Research Article

Crystal structure of the τ_{11} $Al_4Fe_{1.7}Si$ phase from neutron diffraction and ab initio calculations

Biswas Rijal[a], Sujeily Soto[a], Kausturi Parui[a], Anil Sachdev[b], Megan M. Butala[a], Michele V. Manuel[a], Richard G. Hennig[a]

[a] Material Science and Engineering, University of Florida, Gainesville, FL 32611, USA
[b] General Motors Research & Development, Warren, MI, USA

ARTICLE INFO

Article history:
Received 19 July 2021
Received in revised form 17 November 2021
Accepted 4 December 2021
Available online 13 December 2021

Keywords:
Intermetallics
Crystal structure
Density functional theory
Neutron diffraction
Rietveld refinement
Al-Fe-Si

ABSTRACT

The intermetallic τ_{11} $Al_4Fe_{1.7}Si$ phase is of interest for high-temperature structural application due to its combination of low density and high strength. We determine the crystal structure of the τ_{11} phase through a combination of powder neutron diffraction and density functional theory calculations. Using Pawley and Rietveld refinements of the neutron diffraction data provides an initial crystal structure model. Since Al and Si have nearly identical neutron scattering lengths, we use density-functional calculations to determine their preferred site occupations. The τ_{11} phase exhibits a hexagonal crystal structure with space group $P6_3/mmc$ and lattice parameters of $a = 7.478$ Å and $c = 7.472$ Å. The structure comprises five Wyckoff positions; Al occupies the 6*h* and 12*k* sites, Fe the 2*a* and 6*h* sites, and Si the 2*a* sites. We observe site disorder and partial occupancies on all sites with a large fraction of 80% Fe vacancies on the 2*d* sites, indicating an entropic stabilization of the τ_{11} phase at high temperature.

1. Introduction

Al-Fe based compounds possess high melting points, high hardness, low density, low cost, and good oxidation and corrosion resistance, making them highly attractive structural materials. A high Al content in Al-Fe alloys is desirable for lightweight engine parts to drive high power densities and excellent transient engine performance [1]. However, the mechanical properties of the Al-Fe compounds tend to decrease with increasing Al content. The application of high Al-content Al-Fe intermetallic compounds is especially limited by their brittleness. For example, the compressive strain drops rapidly from 0.8% at 560 MPa (Fe_3Al, face-centered cubic structure) to 0% at 200 MPa ($FeAl_3$, monoclinic structure) [1].

However, the addition of Si into an Al-Fe binary system stabilizes a crystal structure with low density and improved mechanical properties. The Al-Fe-Si ternary phase space is complex, consisting of at least 11 equilibrium ternary phases and 19 invariant reactions [2]. In addition, at least 5 metastable ternary phases have been reported [3]. $Al_4Fe_{1.7}Si$, known as τ_{11}, holds great promise for structural applications as a result of its low theoretical density, about 4.1 g/cm^3, unique hexagonal crystal structure and an estimated tensile strength of 1500 MPa [4,5].

For the Al-Fe-Si system, x-ray and neutron diffraction cannot easily distinguish between Al and Si due to their similar x-ray form factor and neutron scattering length. Therefore, we combine a refinement of experimental neutron diffraction data with density functional theory (DFT) calculations. Fig. 1(a) illustrates that the previously reported crystal structure of the τ_{11} intermetallic phase based on x-ray diffraction [6] assumed a mixed occupancy of Al and Si with the ratio given by the overall composition and partial occupancy of Fe. The 2*a*, 6*h*, and 12*k* Wyckoff sites have 80% Al and 20% Si occupancies and the 2*d* site has a partial occupancy of 45% Fe. Computational methods provide an opportunity to determine the energy of different site occupancies.

In this work to better understand and model the properties of the τ_{11} phase, we combine a refinement of experimental neutron diffraction data with density functional theory (DFT) calculations to investigate the structure and site occupancies. The results reveal a different atomic structure than that previously reported and identify preferred Al occupancy on the 6*h* and 12*k* sites and Si occupancy on the 2*a* site. In our experimental approach, while the lattice constants and symmetry of the published structure reproduced the positions of peaks in diffraction data, considerable changes in atomic positions were required to model peak intensities. DFT calculations confirm that this structure has an energy 250 meV/atom lower than the previously published model. Noteworthy, we obtained the

E-mail address: rhennig@ufl.edu (R.G. Hennig).

https://doi.org/10.1016/j.jallcom.2021.163141
0925-8388/

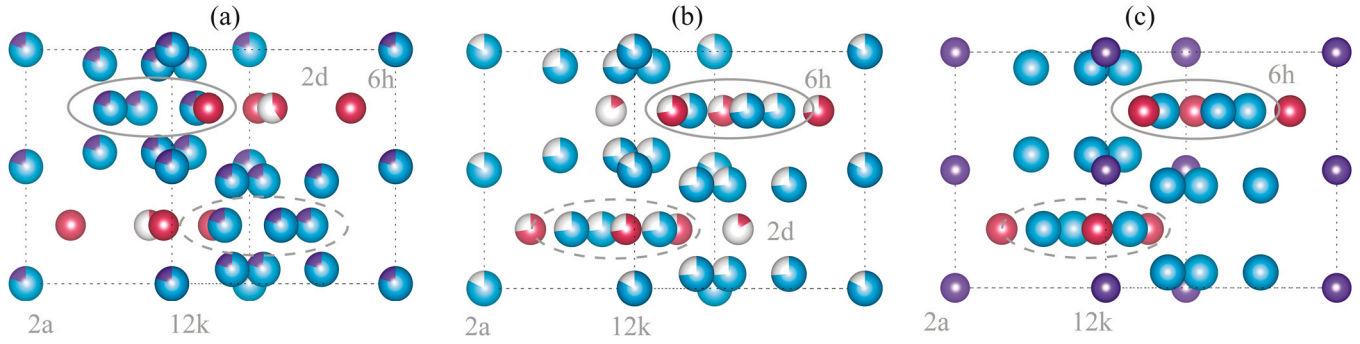

Fig. 1. The crystal structure of the τ_{11} phase from (a) Ref. [6], (b) the neutron diffraction refinement, and (c) the DFT relaxations. The aqua, purple, and red spheres denote Al, Si, and Fe, respectively. Two colors in a sphere indicates mixed occupancy of two atomic species, and white partial occupancy depicts partial occupation of a site. Partial occupancy used in DFT calculations in the different sites were motivated by experimentally observed probabilities. The Wyckoff positions are labeled, and the ellipses indicate the shift in the Al2 (6*h*) sites along the *y* coordinate between the previous refinement and this work. Three tables below denote the atomic positions and occupancies of the three models, i.e., Ref. [6], the Rietveld refinement, and DFT relaxations.

experimental and computational structural models independently, initializing the refinement and structural relaxation in each approach with the atomic positions of the published structure (Fig. 1(b) and (c)). In addition to consistency from parallel approaches, the resulting structure is more intuitive, with a more homogeneous distribution of atoms across the structure. This improved atomic structure model enables future alloy design studies to improve the high-temperature thermodynamics stability, identify optimal synthesis conditions, and enhance the mechanical properties of τ_{11}.

2. Methods

2.1. Synthesis

Al-Fe-Si ternary alloys with nominal compositions of $Al_{64.0}Fe_{25.0}Si_{11.0}$ and $Al_{63.0}Fe_{25.5}Si_{11.5}$ were fabricated by arc melting 99.99 wt% Al and 99.98 wt% Fe from Sigma Aldrich with an Al-50 wt% Si alloy from Belmont Metals under an argon atmosphere. The melting was repeated 5 times to ensure homogenization of the alloys. Then the alloys were annealed at 950 °C for 100 h. In order to protect the samples from oxidation at high temperatures, each alloy was individually wrapped inside VakPak65 heat treating containers. After the heat treatments, the containers with the samples inside were quickly removed from the furnace and quenched in water. A Tescan MIRA3 scanning electron microscope (SEM) coupled with an EDAX Octane Pro energy dispersive spectrometer (EDS) was used to measure the chemical composition of the alloys. The average of at least three points were measured to obtain the compositions.

2.2. Neutron diffraction and analysis

Alloy samples were ground into fine powders for neutron diffraction experiments. The neutron powder diffraction (NPD) was measured at HFIR-HB2A at Oak Ridge National Laboratory. The measurements were performed at room temperature with a constant wavelength of 1.54 Å over an $8° < 2\theta < 154°$ range.

For the NPD data analysis, GSAS-II [7] and Topas Academic v6 [8] software were used for initial LeBail and Pawley fits. Lattice and instrumental parameters from these fits were used in the subsequent Rietveld refinement of the full unit cell details of lattice parameters, atomic positions, atomic displacement parameters, and site occupancies. Since the scattering lengths densities of Al of 2.078×10^{-6} Å^{-2} and Si of 2.074×10^{-6} Å^{-2} are nearly identical, we used a single species on sites that realistically have mixed occupancy of Al and Si. The resulting error in the structure factor from this simplification is minor and reduces the number of free parameters to give a more meaningful fit.

2.3. Computation

We used DFT energies of various configurations to distinguish the site occupation for Si and Al, which is not resolved by diffraction alone. The computational prediction of the ground state structure for a given composition involves finding the structure or set of structures with the lowest formation energy at that composition. We construct the convex hull of the energies for the known and calculated Al-Fe-Si phases to compare the energy of structures with different compositions and identify the most stable site occupations. The convex hull is defined as the set of points that encloses all the points in the set. The enclosing points can be used to determine the lowest energy structure. For the convex hull, lines and planes connect the lowest energy phases and represent the system's energy at 0 K. Configurations with energies above the convex hull are unstable. The distance from the hull for various structures indicates the relative stability of those structures.

The structural relaxation and energy calculations were performed with the plane-wave DFT code VASP [9–12] using the PBE functional [13] and the projector augmented wave method [14,15]. The cutoff energy for the plane wave basis set was set to 450 eV with a *k* point density of 1000 points per reciprocal atom. We used very tight convergence criteria for the structure relaxations. All structures were relaxed until the energy difference between subsequent electronic steps was less than 0.001 meV and between the ionic relaxation steps the difference was less than 0.01 meV.

3. Results and discussion

3.1. Energy minimization

To create the convex hull, we obtain the crystal structures of all potentially competing phases for τ_{11}-$Al_4Fe_{1.7}Si$ from the Inorganic Crystal Structure Database (ICSD) [16] and the Materials Project database [17–19]. We do not consider the disorder in the competing phases and used the crystal structures as provided by the Materials Project database. Then, we relax all the structures and calculate their energies. The considered Al-Fe-Si phases include the elemental phases of Al, Fe, and Si, and 12 binary and 36 ternary compounds. The crystal structure of τ_{11}-$Al_4Fe_{1.7}Si$ (initially called τ_{10}) from German et al. [6] exhibits a hexagonal unit cell of the Co_2Al_5-type structure with 28 atoms, space group $P6_3/mmc$, and lattice parameters $a = 7.509$ Å and $c = 7.594$ Å. The 2*a*, 6*h*, and 12*k* Wyckoff sites are partially occupied by a mixture of Al and Si, and Fe occupies the 6*h* and, partially, the 2*d* sites.

Fig. 2 a, b shows the change in hull distance between the lowest energy structure and the structures with site substitution in 2*a*, 6*h*,

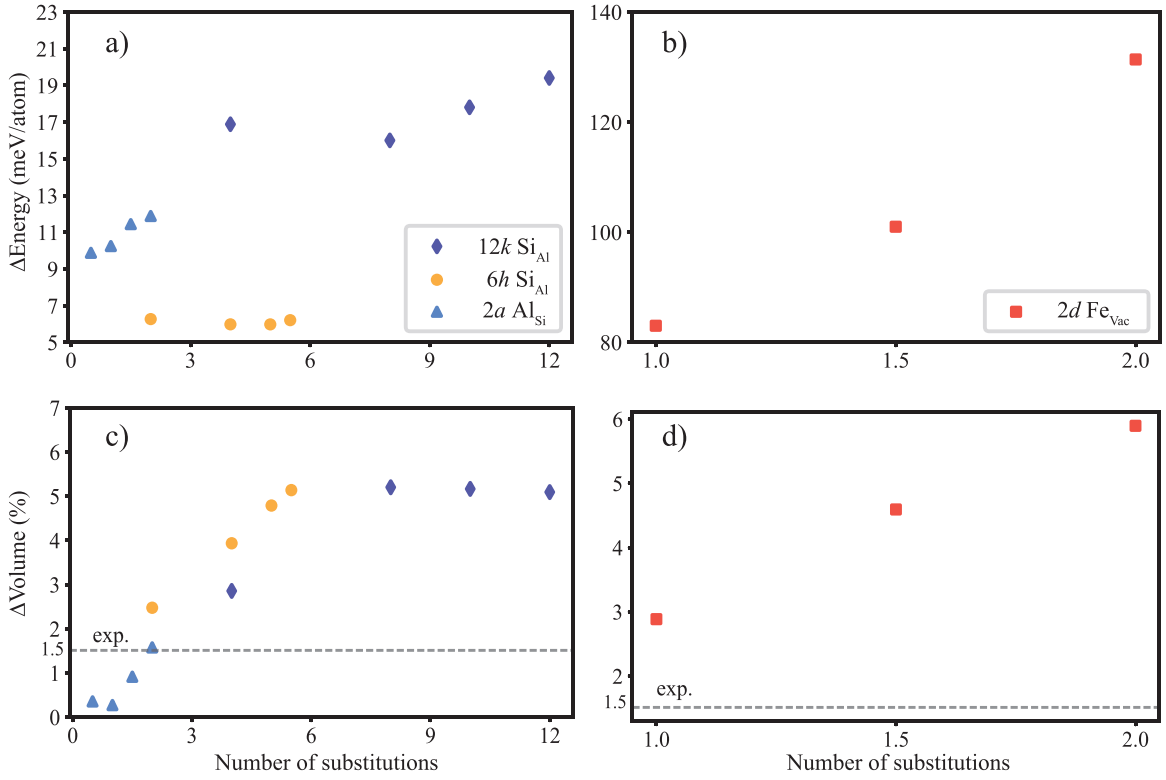

Fig. 2. (a, b) Change in energy for various site substitutions relative to the τ_{11}-$Al_4Fe_{1.7}Si$ structure with the lowest energy. The energy, E_{hull} in meV/atom is measured by the distance from the convex hull obtained from all possible competing phases of the τ_{11} phase. (c, d) Percentage change in volume of the various choices of site occupancy for the τ_{11}-$Al_4Fe_{1.7}Si$ structure and the lowest energy structure. The dashed line represents the experimental volume obtained from the refinement. The symbols in all the figure represent the substitution in a Wyckoff substitution.

12*k*, and 2*d* Wyckoff sites by Al, Fe, and Si. The energies are obtained from DFT energies relative to the convex hull of competing phases. In the DFT convex hull, the competing phases for the τ_{11} phase are $Al_{26}Fe_9Si_6$, $Al_{13}Fe_4$ and $Al_2Fe_3Si_3$.

The DFT calculations provide the insight into occupational disorder on the Wyckoff sites. The refinement cannot resolve the occupation of the 2*a*, 12*k*, and 6*h* Wyckoff sites by Al and Si and indicates a small partial occupancy of the 2*d* site by Fe. The hull distance is smallest when Si occupies the 2*a* sites, Al the 12*k* and 6*h* sites, and the 2*d* site is empty. The energy cost for Al occupying a 2*a* site is about 10 meV/atom. The energy cost for a Si atom replacing Al on one of the 6*h* sites is about 10 meV/atom, and for the 12*k* site, it is slightly higher at about 20 meV/atom. This indicates that Si preferentially occupies the 2*a* and Al the 6*h* and 12*k* Wyckoff sites. For the 2*d* site, occupying it by Fe increases the energy by about 100 meV/atom, indicating that the 2*d* site will be preferentially empty even at high temperatures, consistent with the diffraction analysis by German et al. [6]. The small energy cost for Al/Si occupational disorder indicates that configurational disorder stabilizes the τ_{11} phase at high temperatures and that Si preferentially occupies the 2*a*, Al the 6*h* and 12*k*, and Fe the other 6*h* site, while the 2*d* site is preferentially empty.

In addition to the energy, we also compare the Wyckoff positions and lattice parameters of the different configurations with the experimental ones. Most Wyckoff positions are very similar between the DFT relaxed structure and the structure by German et al. However, we find a large shift of the Al atoms in the 6*h* position by close to 1Å along the *y*-axis, which is illustrated in Fig. 1. As shown below, this change in position is consistent with our neutron diffraction data. For the lattice parameter, German et al. [6] obtained $a = 7.509$ Å and $c = 7.594$ Å. For the lowest energy structure shown in Fig. 1(c), we obtain similar values of $a = 7.478$ Å and $c = 7.472$ Å. Fig. 2c, d shows the change in volume of the unit cell due to site occupancies. The experimental volume is 1.5% larger than the DFT calculated volume for the lowest energy structure. We observe that the volume shows larger changes when Si substitutes Al in the 6*h* and 12*k* positions. Likewise, the change in volume is between 3% and 5% when Fe occupies the vacancy in the 2*d* position. Since the PBE functional typically overestimates the volume, the increase in volume by about 3–5% percent due to Al/Si disorder on the 6*h* and 12*k* sites and Fe/vacancy disorder on the 2*d* sites is consistent with the DFT results.

Thus, the DFT calculations show that the τ_{11} phase has the lowest energy with an ordering of Al and Si such that Al occupies the 12*k* and 6*h* positions and Si the 2*a* position, and Fe occupying another 6*h* site. In addition, our calculations indicate that a vacant 2*d* position is energetically favorable. Therefore, DFT predicts the lowest energy τ_{11} structure with 18 Al, 6 Fe, and 2 Si atoms in 6*h* and 12*k*, 2*d*, and 2*a* positions, respectively. The predicted lattice parameters match the published structure. However, there is a significant shift of 1 Å in the 6*h* position compared to the published structure. Therefore, we conducted a neutron diffraction study of the τ_{11} structure to validate the DFT results. In this study, we were concerned with determining the lowest energy crystal structure and neglect the role of entropy on the disorder at higher temperatures.

3.2. Structure refinement

Given the considerable difference between the lowest energy structure we identified with DFT and that previously published, we refined the atomic structure model (beginning with the published structure) against experimental data obtained from NPD. EDS measurements at various points gave a mean composition of 64.7 at% Al, 25.1 at% Fe and 10.3 at% Si (and the relevant error/standard deviation) as shown in Table 1. DFT calculated the lowest energy structure for the τ_{11} phase with 69.23 at% Al, 23.07 at% Fe 7.69 at% Si. The NPD

Table 1
Composition obtained from EDS micrograph in atomic percent with standard deviation inside the parenthesis.

Nominal phase composition			Measured phase composition		
Al	Fe	Si	Al	Fe	Si
64	25	11	64.7	25.1	10.3

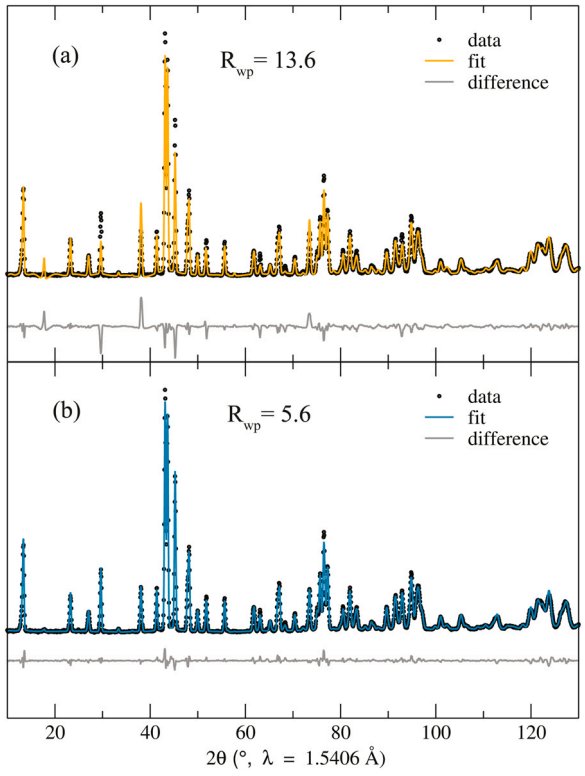

Fig. 3. Comparative plots of data, fit and difference curve with Fe on the original (a) vs. refined site (b). Neutron diffraction data (dots) are fitted (orange and blue) using Rietveld refinement. The difference (black) line shows the difference between the actual data and the fit. Correcting the Fe site significantly improves the goodness of from R_{wp} = 13.6 to R_{wp} = 5.6.

pattern shown in Fig. 3 has the peak positions that could be matched to the expected reflections for the published τ_{11} phase, confirming the single phase microstructure observed in the SEM image.

During initial Rietveld refinement (using GSAS-II), we found a considerable mismatch between the peak intensities of the published structure and our NPD data. With the various parameters in the unit cell, particularly the mixed and partial site occupancies and degrees of freedom on several atomic position, we were initially in a local least squares minima, preventing us from capturing the relevant structural details. Throughout this effort, peak mismatch, and a high $R_{wp} > 20$ persisted, indicating a substantial difference between our initial model (based on the published structure) and that of our sample.

This initial pass indicated that while the symmetry and lattice parameters, which give rise to the peak positions, were correct, we would need to refine the unit cell model to capture peak intensities. To confirm our lattice parameters and determine instrumental parameters, we performed a Pawley refinement (using Topas). Pawley refinement is a structure-free approach that generates d-spacings based on the lattice parameters and Miller indices, and modifies these to match peak position. However, with Pawley fitting, the intensity of each peak comes from a unique parameter, with no tie to a structural parameter.

In contrast, in the Rietveld refinement, the complete unit cell (lattice parameters, occupancies, atomic displacement parameters, and, particularly, atomic positions) is refined and the positions and identities of atoms in the structural model are used to calculate peak intensities in the fit profile. Beginning with the lattice and instrument parameters (e.g., low angle peak asymmetry correction, zero-offset, etc.) from Pawley refinement and the atomic positions and occupancies from the published structure, we again saw significant peak intensity mismatch in Rietveld fitting, as expected.

Before refining atomic positions, occupancies, and atomic displacement parameters (B_{eq}), we modified the unit cell to reduce the number of correlated parameters. In particular, we simplified our model based on the mixed Al and Si occupancy on 2*a*, 6*h*, and 12*k* sites [6]; in particular, given their nearly identical scattering lengths (2.078×10^{-6} Å^{-2} for Al and 2.074×10^{-6} Å^{-2} for Si), these species cannot be distinguished using typical diffraction methods. As such, there was no physical insight to draw from refining their relative occupancies in the structure. Accordingly, we modeled the mixed Al–Si sites as occupied by only Al (Si alone would produce functionally equivalent results). The resulting error in the structure factor from this simplification was be minor and resulted in a more meaningful fit with fewer correlated parameters.

The fit improved upon refining the lattice parameters, atomic positions, occupancies, and isotropic displacement parameters (B_{eq}), yielding an R_{wp} of 13.6 (Fig. 3a). The most considerable difference between the model and the experimental data was in the *y* positions of Al2 (on a 12*k* site), which is in agreement with the atomic position identified by DFT. In the interest of, again, a more homogeneous distribution of atoms in the unit cell, we shifted Fe1 to an alternate 2*d* site, with $z = \frac{3}{4}$ rather than $\frac{1}{4}$. In combination with the refinement of a Gaussian strain parameter, which improved the peak shape fit at high angles, this change in Fe1 position resulted in excellent agreement between the data and the structural model, reflected in an R_{wp} of 5.2 (Fig. 3b). The final positions and occupancies from this fit are detailed in Fig. 1 and, aside from a second and low occupancy Fe site, shows excellent agreement with the lowest energy structure identified from DFT.

To ensure the physical relevance of our refined model, particularly the resulting atomic ratios, we used the occupancies and site multiplicities to compare the ratio of main group elements (Al + Si) and Fe, since the ratios of Al and Si could not be individually refined in the model. The resulting (Al + Si)/Fe ratios from the refinement and the experimentally measured composition are 3.2 and 3.0 respectively. This confirms the physical relevance of the refined structure.

Our calculated and refined structures have a *c*/*a* ratio of 0.99 and a density of 4.02 g/cm^3, which are lower than those of pure Ti metal, with a *c*/*a* ratio of 1.588 and a density of 4.55 g/cm^3 [20]. The packing fraction of the predicted structure is 0.77 indicating it has a very closed packed structure. Primary differences from the published structure are in the positions of Al/Si atoms in *y* for the 6*h* Wyckoff positions (Fig. 1a and b) and the absence of Fe atoms in 2*d* Wyckoff sites.

4. Conclusion

Through the combination of DFT calculations and Rietveld refinement of neutron diffraction data, we determined a revised structure of the τ_{11}-$Al_4Fe_{1.7}Si$ intermetallic phase. The most significant change is the shift in the positions of the Al/Si 6*h* position, which was consistently identified in the neutron diffraction refinement and the DFT calculations, reducing the energy by 260 meV compared to the previously reported structure [6]. Since the neutron scattering length of Al and Si are nearly indistinguishable, we used DFT calculations to identify preferential site occupations. Based on

the DFT energies, we predict that Al and Si are disordered and that Al prefers the 6*h* and 12*k* sites and Si the 2*a* site. The observation of a large fraction of Fe vacancies and the Al/Si disorder indicates an entropic stabilization of the τ_{11}-$Al_4Fe_{1.7}Si$ phase at high temperature.

From a chemical perspective, the new structure is more intuitive, with a more homogeneous distribution of density across the unit cell. This improved structural model retains its *c*/*a* ratio with highly closed packed structure. Further, variations of the structure and computational prediction of their properties are enabled, allowing improved determination of structure-property relationships and property prediction. Studies can be conducted to increase the phase stability region for τ_{11} with quaternary addition to enable alloys that are still low cost, low density, and suitable for high temperature applications, replacing more costly Ti-based alloys. Our results additionally highlight the utility of modern diffraction and structural modeling algorithms to advance structure-property understanding of metal alloys.

5. Disclaimer

This report was prepared as an account of work sponsored by an agency of the United States Government. Neither the United States Government nor any agency thereof, nor any of its employees, makes any warranty, express or implied, or assumes any legal liability or responsibility for the accuracy, completeness, or usefulness of any information, apparatus, product, or process disclosed, or represents that its use would not infringe privately owned rights. Reference herein to any specific commercial product, process, or service by trade name, trademark, manufacturer, or otherwise does not necessarily constitute or imply its endorsement, recommendation, or favoring by the United States Government or any agency thereof. The views and opinions of authors expressed herein do not necessarily state or reflect those of the United States Government or any agency thereof.

CRediT authorship contribution statement

All authors contributed extensively to the work presented in this paper. **Biswas Rijal**, **Sujeily Soto**, **Anil Sachdev**, **Michele Manuel**, and **Richard Hennig** conceived the overall synthesis, diffraction, and computational study methodology. **Sujeily Soto** and **Michele Manuel** performed the materials synthesis. **Kausturi Parui** and **Megan M. Butala** performed the neutron refinement. **Biswas Rijal** and **Richard Hennig** performed the calculations and computational analysis. All authors contributed to the writing of the manuscript.

Declaration of Competing Interest

The authors declare that they have no known competing financial interests or personal relationships that could have appeared to influence the work reported in this paper.

Acknowledgement

This materials is based upon work supported by the U.S. Department of Energy (DOE), Office of Energy Efficiency and Renewable Energy (EERE), specifically the Vehicle Technologies Office under Award no. DE-EE0007742. A portion of this research used resources at the High Flux Isotope Reactor, a DOE Office of Science User Facility operated by Oak Ridge National Laboratory. The authors are thankful to Dr. Andrew Bobel at General Motors (GM) for valuable discussions.

References

[1] Chain Tsuan Liu, Robert Wolfgang Cahn, Gerhard Sauthoff, Ordered Intermetallics: Physical Metallurgy and Mechanical Behaviour, 213 Springer Science & Business Media, 2012.
[2] Yong Du, Julius Clemens Schuster, Zi-Kui Liu, Rongxiang Hu, Philip Nash, Weihua Sun, Weiwei Zhang, Jiong Wang, Lijun Zhang, Chengying Tang, et al., A thermodynamic description of the al-fe-si system over the whole composition and temperature ranges via a hybrid approach of calphad and key experiments, Intermetallics 16 (4) (2008) 554–570.
[3] G. Ghosh, Aluminium–iron–silicon, Iron Systems, Part 1, (2008).
[4] Seong Woo Kim, Un Ho Im, Hyeong Cheol Cha, Se Hyeong Kim, Ji Eun Jang, Ki Young Kim, Removal of primary iron rich phase from aluminum-silicon melt by centrifugal separation, China Foundry 10 (112) (2013) 117 2013.
[5] Zhongyi Liu, Anil K. Sachdev, Rapidly solidified high-temperature aluminum iron silicon alloys, 2019, US Patent 10,435,773.
[6] N.V. German, V.K. Belsky, T.I. Yanson, O.S. Zarechnyuk, Crystal-structure of $Fe_{1.7}Al_4Si$, 1989.
[7] Brian H. Toby, Robert B. Von Dreele, GSAS-II: the genesis of a modern open-source all purpose crystallography software package, J. Appl. Crystallogr. 46 (2) (2013) 544–549.
[8] Alan A. Coelho, TOPAS and TOPAS-academic: an optimization program integrating computer algebra and crystallographic objects written in C++, J. Appl. Crystallogr. 51 (1) (2018) 210–218.
[9] Georg Kresse, Jürgen Hafner, Ab initio molecular dynamics for liquid metals, Phys. Rev. B 47 (1) (1993) 558.
[10] Georg Kresse, Jürgen Hafner, Ab initio molecular-dynamics simulation of the liquid-metal-amorphous-semiconductor transition in germanium, Phys. Rev. B 49 (20) (1994) 14251.
[11] Georg Kresse, Jürgen Furthmüller, Efficient iterative schemes for ab initio total-energy calculations using a plane-wave basis set, Phys. Rev. B 54 (16) (1996) 11169.
[12] Georg Kresse, Jürgen Furthmüller, Efficiency of ab-initio total energy calculations for metals and semiconductors using a plane-wave basis set, Comput. Mater. Sci. 6 (1) (1996) 15–50.
[13] John P. Perdew, Kieron Burke, Matthias Ernzerhof, Generalized gradient approximation made simple, Phys. Rev. Lett. 77 (18) (1996) 3865.
[14] Peter E. Blöchl, Projector augmented-wave method, Phys. Rev. B 50 (24) (1994) 17953.
[15] Georg Kresse, Daniel Joubert, From ultrasoft pseudopotentials to the projector augmented-wave method, Phys. Rev. B 59 (3) (1999) 1758.
[16] I Levin, Nist inorganic crystal structure database (icsd), 2018.
[17] Shyue Ping Ong, Lei Wang, Byoungwoo Kang, Gerbrand Ceder, Li-Fe-P-O_2 phase diagram from first principles calculations, Chem. Mater. 20 (5) (2008) 1798–1807.
[18] Anubhav Jain, Geoffroy Hautier, Shyue Ong, Charles Moore, Christopher Fischer, Kristin Persson, Gerbrand Ceder, Formation enthalpies by mixing GGA and GGA + U calculations, Phys. Rev. B 84 (4) (2011) 045115.
[19] Anubhav Jain, ShyuePing Ong, Geoffroy Hautier, Wei Chen, William Davidson Richards, Stephen Dacek, Shreyas Cholia, Dan Gunter, David Skinner, Gerbrand Ceder, Kristin a. Persson, The materials project: a materials genome approach to accelerating materials innovation, APL Mater. 1 (1) (2013) 011002.
[20] Dirk J. Oh, Robert A. Johnson, Relationship between *ca* ratio and point defect properties in HCP metals, J. Nucl. Mater. 169 (1989) 5–8.